Supplementary Information for

Degradation of Atrazine in the Electrochemical LED-UV_{275nm}/Cl_2 System: The Role of $^{\bullet}OH$ and $Cl^{\bullet}$

Ying Huang[1,#], Yangyang Li[1,#], Minghao Kong[2], Dionysios D. Dionysiou[2*], and Lecheng Lei[1,3*]

[1]Key Laboratory of Biomass Chemical Engineering of Ministry of Education, College of Chemical and Biological Engineering, Zhejiang University, Hangzhou 310027, China

[2]Department of Chemical and Environmental Engineering, University of Cincinnati, Cincinnati, Ohio 45221, United States

[3]Institute of Zhejiang University - Quzhou, Quzhou, 32400, China

*Corresponding Authors: Dionysios D. Dionysiou & Lecheng Lei

e-mail: dionysios.d.dionysiou@uc.edu & leilc@zju.edu.cn.

# Contributed equally to this work.

Contents

Table S1. Primary parameters of the synthetic RO concentrate.

	Units	Synthetic RO concentrate
pH		7.8
Conductivity	$\mu S\ cm^{-1}$	3275
UV_{275nm} absorption	cm^{-1}	0.82
DOC	$mg\ L^{-1}$	15
Cl^-	mM	28.6
NH_4^+	mM	1.6
SO_4^{2-}	mM	15.3

Table S2. Rate constants used in this work.

	$k_{\cdot OH}$	$k_{O^{\bullet -}}$	$k_{Cl^{\bullet}}$	$k_{Cl_2^{\bullet -}}$	$k_{chlorine}$	k_{EC}	$k_{UV275nm}$
	(M^{-1} s^{-1})	(M^{-1} s^{-1})	(M^{-1} s^{-1})	(M^{-1} s^{-1})	(L mg^{-1} s^{-1})	(s^{-1})	(s^{-1})
ATZ	3.0×10^9 [1]	-	6.9×10^9 [2]	-	1.5×10^{-6}	2.5×10^{-5}	4.9×10^{-5}
NB	3.9×10^9 [3]	-	-	-	3.5×10^{-7}	2.4×10^{-6}	4.7×10^{-6}
MeOH	9.7×10^8 [3]	7.5×10^8 [3]	-	-	-	-	-
t-BuOH	6.0×10^8 [4]	-	3.0×10^8 [4]	700 [2]	-	-	-
IBP	7.0×10^9 [5]	-	2.8×10^{10} [5]	$< 5 \times 10^6$ [5]	-	-	-
CBZ	8.8×10^9 [5]	-	3.3×10^{10} [5]	0.4×10^8 [5]	-	-	-
DCF	9.0×10^9 [6]	-	3.8×10^{10} [5]	1.2×10^9 [5]	-	-	-

EC: direct electro-oxidation; ATZ: atrazine; NB: nitrobenzene; MeOH: methanol; t-BuOH: tert-butanol; IBP: ibuprofen; CBZ: carbamazepine; DCF: diclofenac.

Table S3. Detected transformation products of atrazine in UV-EC/Cl_2 and EC/Cl_2.

Reaction conditions: $[atrazine]_0$ = 20 μM, $[Cl^-]_0$ = 20 mM, 10 mM phosphate buffer (pH = 7.0), anodic potential = 1.5 V *vs.* Ag/AgCl, average UV_{275nm} fluence rate = 0.25 mW cm^{-2}.

	RT (min)	$[M-H]^-$		Chemical Formula	Proposed Structure	Detected	
		Theoretical *m/z*	Observed *m/z*			EC/Cl_2	UV_{275nm}-EC/Cl_2
ATZ	5.6	216.101	216.101	$C_8H_{14}ClN_5$	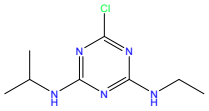	√	√
TP_{146}	2.0	146.023	146.024	$C_3H_4ClN_5$	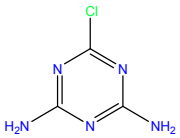	√	√
TP_{170a}	1.7	170.104	170.104	$C_6H_{11}N_5O$	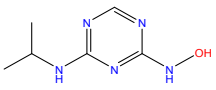	×	√
TP_{170b}	2.3				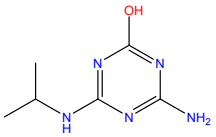	√	√
TP_{172}	2.2	172.038	172.038	$C_5H_6ClN_5$	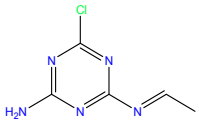	√	√
TP_{174} (DIA)	3.0	174.054	174.056	$C_5H_8ClN_5$	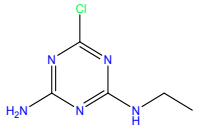	√	√
TP_{188-1}	2.0	188.033	188.033	$C_5H_6N_5OCl$	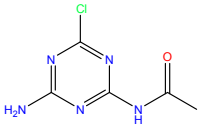	√	√

$TP_{188\text{-}2}$ (DEA)	4.3	188.070	188.070	$C_6H_{10}ClN_5$	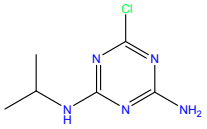	√	√
TP_{198}	2.9	198.135	198.136	$C_8H_{15}N_5O$	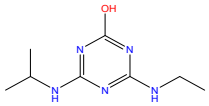	×	√
TP_{212a}	1.7	212.114	212.115	$C_8H_{13}N_5O_2$	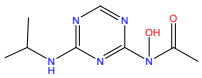	×	√
TP_{212b}	2.3				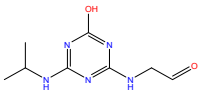	√	√
TP_{214a}	4.1	214.085	214.086	$C_8H_{12}ClN_5$		√	√
TP_{214b}	5.4				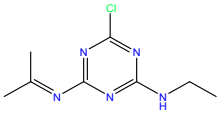	√	√
TP_{216}	3.5	216.065	216.066	$C_7H_{10}N_5OCl$	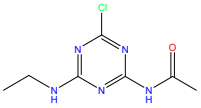	√	√
TP_{230}	4.2	230.080	230.080	$C_8H_{12}ClN_5O$	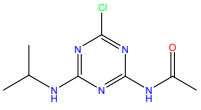	√	√
TP_{232a}	3.7	232.096	232.097	$C_8H_{14}ClN_5O$	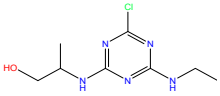	√	√
TP_{232b}	4.2				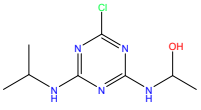	√	√

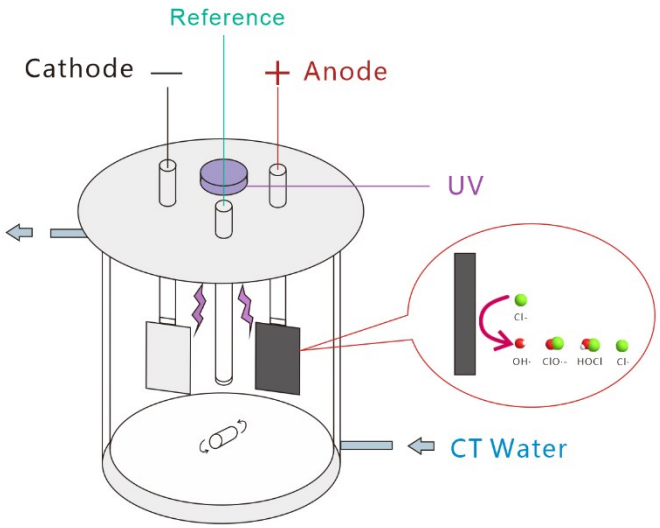

Fig. S1. Photo-electrochemical reactor.

CT water: constant-temperature water; Cathode: a stainless-steel cloth; Anode: RuO_2/IrO_2-Ti plate; Reference: a Ag/AgCl reference electrode (in saturated KCl, 0.199 V *vs*. standard H_2 electrode); UV: LED-UV_{275nm}.

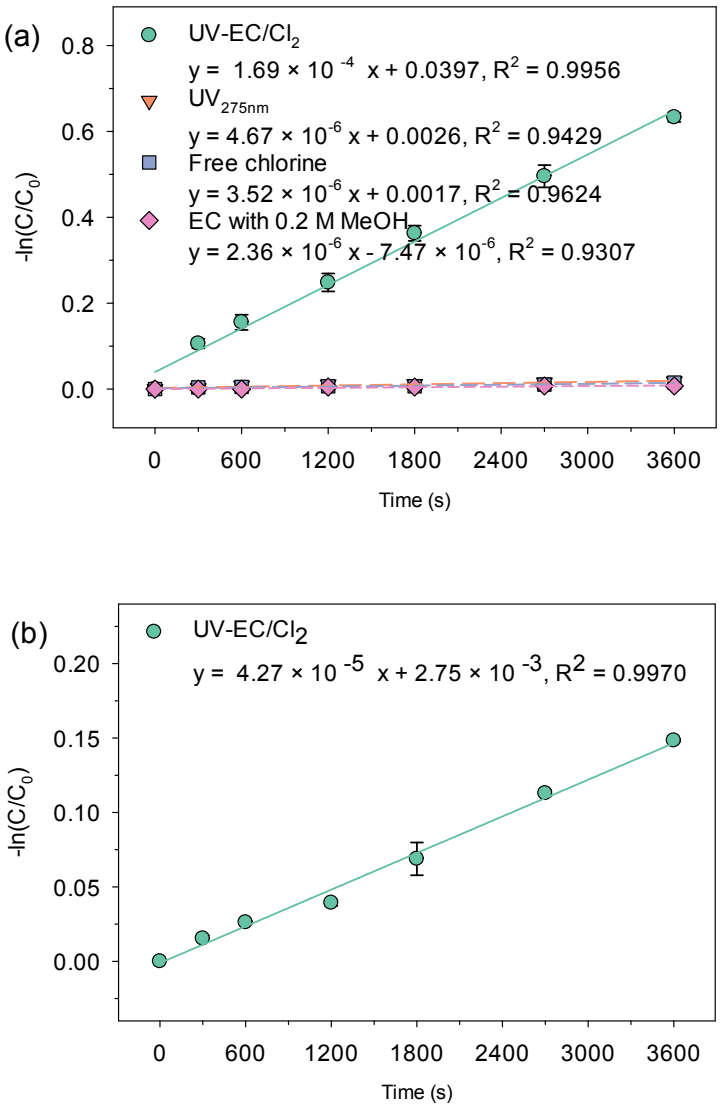

Fig. S2. Degradation of 1μM nitrobenzene (NB) (a) and 20 μM NB (b) by UV-EC/Cl_2, UV_{275nm}, 10 mg L^{-1} free chlorine oxidation, and direct electro-oxidation (EC) with 0.2 M MeOH, for determining the steady-state concentration of •OH.

General reaction conditions: $[Cl^-]_0$ = 20 mM, 10 mM phosphate buffer (pH = 7.0), free chlorine = 10 mg L^{-1}, anodic potential = 1.5 V *vs.* Ag/AgCl, average UV_{275nm} fluence rate = 0.25 mW cm^{-2}.

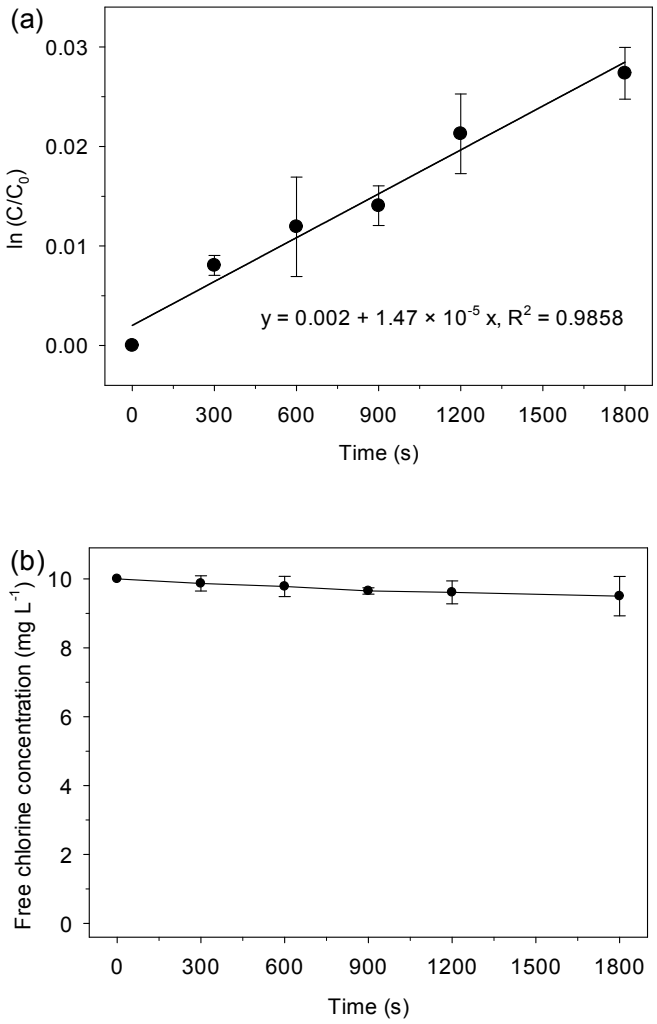

Fig. S3. Reaction of atrazine with chlorine at dark condition (a) and the concentration of chlorine (b). General reaction conditions: $[\text{atrazine}]_0$ = 1 μM, $[\text{chlorine}]_0$ = 10 mg L^{-1}, 10 mM phosphate buffer (pH = 7.0), average UV_{275nm} fluence rate = 0.25 mW cm^{-2}.

The degradation rate of atrazine can be calculated through eq. S1. Since the concentration of chlorine had little change during the chlorination of atrazine, the eq. S1 could be simplified to eq. S3. Thus, the $k_{\text{chlorine, ATZ}}$ was calculated through eq. S3 as 1.5 × 10^{-6} L mg^{-1} s^{-1}.

$$-\frac{d[ATZ]}{dt} = k_{chlorine,ATZ}[chlorine][ATZ] \qquad \text{(eq. S1)}$$

$$-\frac{d[ATZ]}{dt} = k_{chlorine,ATZ} \times 10\ mg\ L^{-1} \times [ATZ] = k_{obs} \times [ATZ] \qquad \text{(eq. S2)}$$

$$k_{chlorine,ATZ} = \frac{k_{obs}}{10\ mg\ L^{-1}} \qquad \text{(eq. S3)}$$

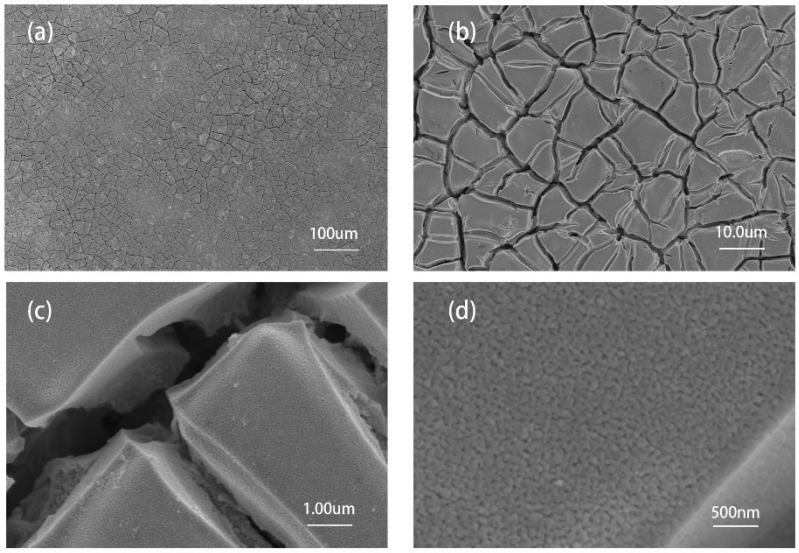

Fig. S4. SEM of the surface of RuO_2-IrO_2-Ti anode at different magnifications (a-d).

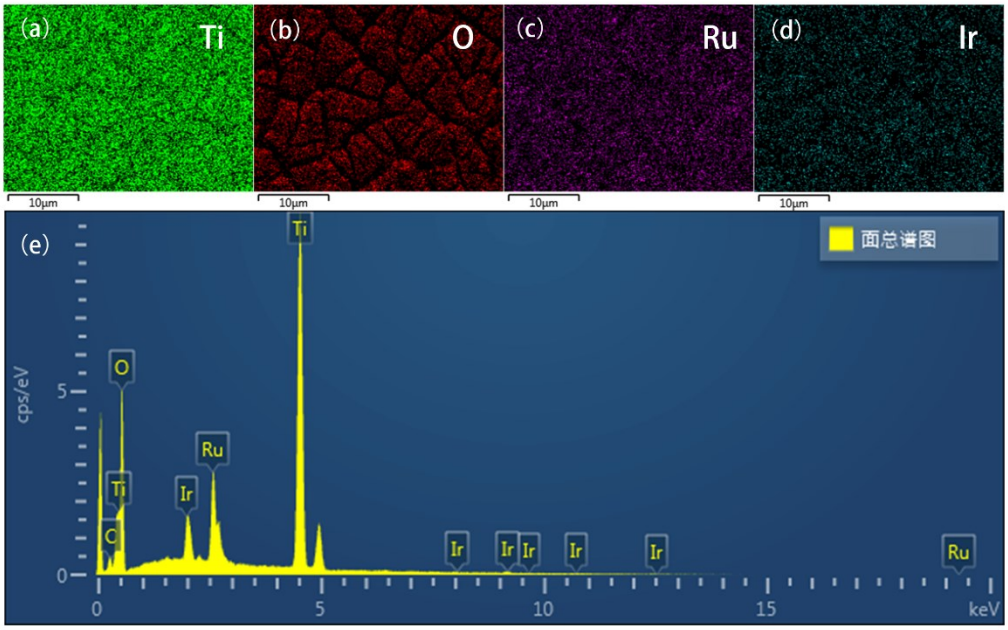

Fig. S5. Element distribution on the surface of RuO_2-IrO_2-Ti anode: (a) Ti, (b) O, (c) Ru, (d) Ir, (e) EDS area total spectrum.

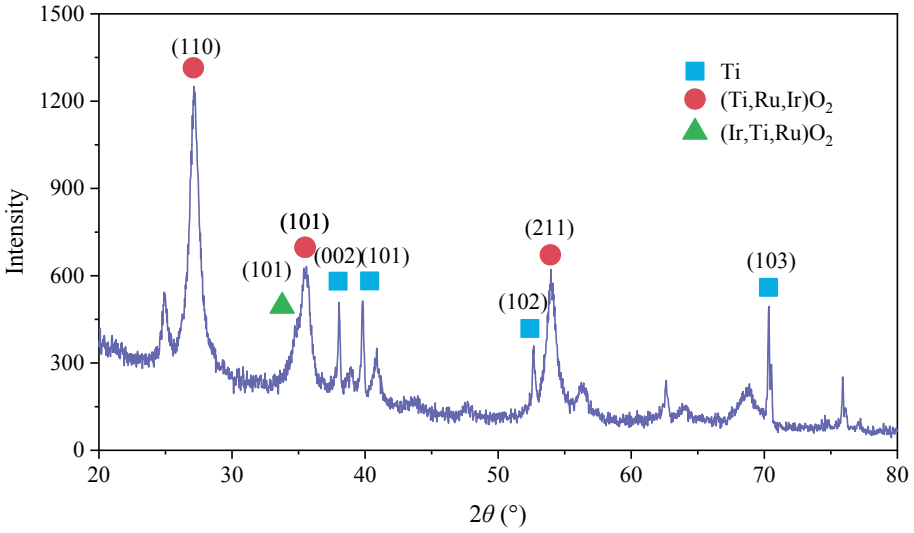

Fig. S6. XRD spectrum of RuO_2-IrO_2-Ti anode.

(Ti,Ru,Ir)O_2 means TiO_2 based solid solution with contents of RuO_2 and IrO_2. (Ir, Ti, Ru)O_2 means IrO_2 based solid solution with contents of TiO_2 and RuO_2.[7]

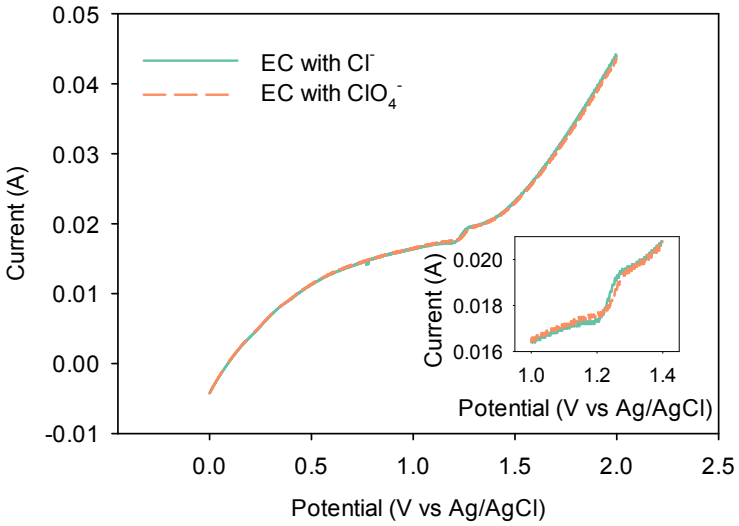

Fig. S7. Liner sweep voltammograms at the RuO_2/IrO_2-Ti electrode with 20 mM Cl^- and ClO_4^- electrolyte (insert was the current change in the potential range of 1.0 to 1.4 V *vs* Ag/AgCl).

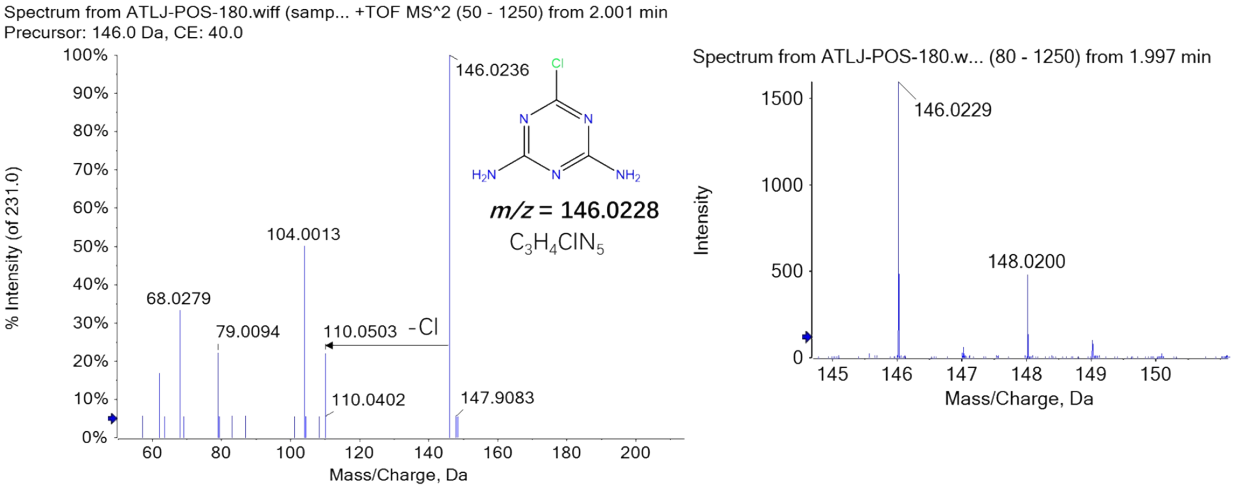
Spectrum from ATLJ-POS-180.wiff (samp... +TOF MS^2 (50 - 1250) from 2.001 min
Precursor: 146.0 Da, CE: 40.0
% Intensity (of 231.0)
Mass/Charge, Da
146.0236
104.0013
68.0279
79.0094
110.0503
-Cl
110.0402
147.9083
m/z = 146.0228
C3H4ClN5
Spectrum from ATLJ-POS-180.w... (80 - 1250) from 1.997 min
Intensity
146.0229
148.0200
Mass/Charge, Da

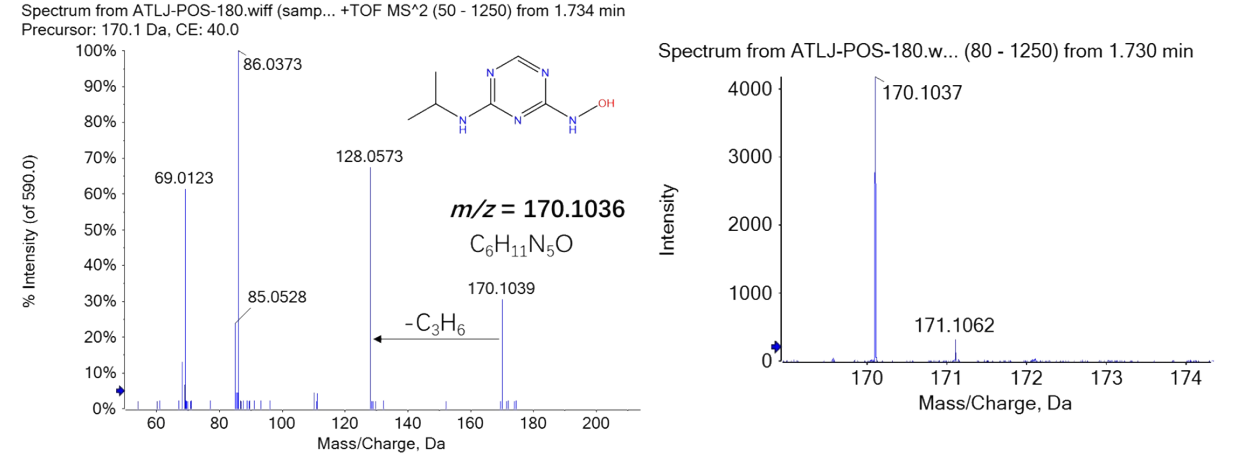
Spectrum from ATLJ-POS-180.wiff (samp... +TOF MS^2 (50 - 1250) from 1.734 min
Precursor: 170.1 Da, CE: 40.0
% Intensity (of 590.0)
Mass/Charge, Da
86.0373
69.0123
128.0573
85.0528
170.1039
-C3H6
m/z = 170.1036
C6H11N5O
Spectrum from ATLJ-POS-180.w... (80 - 1250) from 1.730 min
Intensity
170.1037
171.1062
Mass/Charge, Da

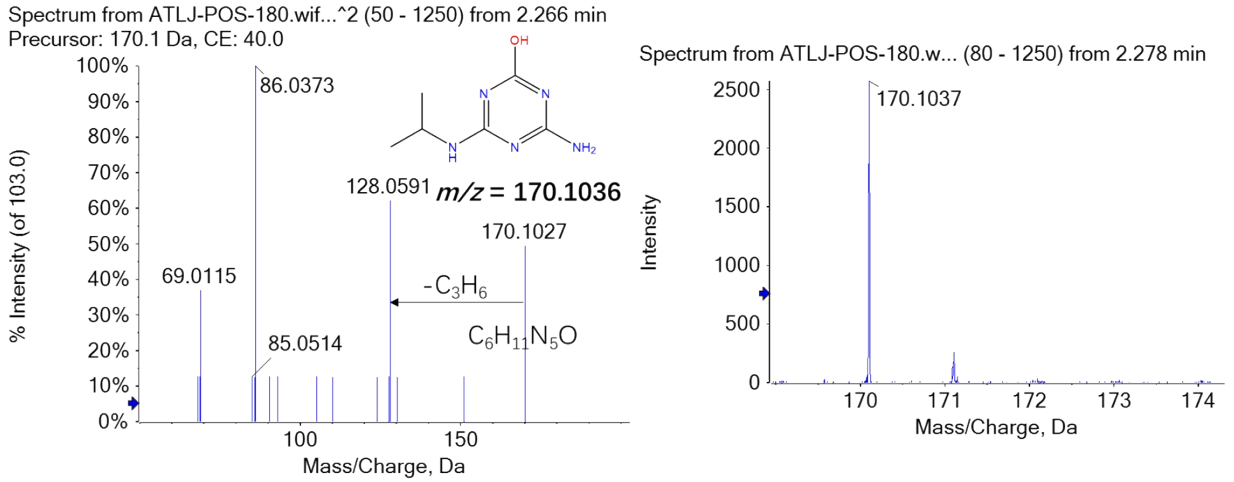
Spectrum from ATLJ-POS-180.wif...^2 (50 - 1250) from 2.266 min
Precursor: 170.1 Da, CE: 40.0
% Intensity (of 103.0)
Mass/Charge, Da
86.0373
128.0591
m/z = 170.1036
170.1027
69.0115
-C3H6
85.0514
C6H11N5O
Spectrum from ATLJ-POS-180.w... (80 - 1250) from 2.278 min
Intensity
170.1037
Mass/Charge, Da

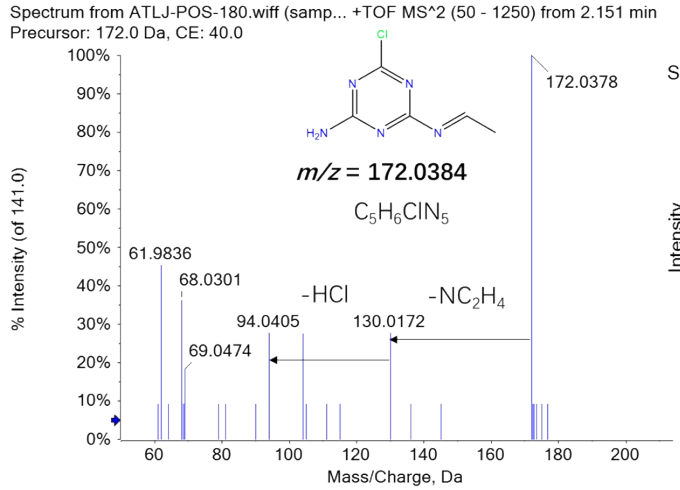
Spectrum from ATLJ-POS-180.wiff (samp... +TOF MS^2 (50 - 1250) from 2.151 min
Precursor: 172.0 Da, CE: 40.0
172.0378
m/z = 172.0384
C5H6ClN5
61.9836
68.0301
-HCl
-NC2H4
94.0405
130.0172
69.0474
% Intensity (of 141.0)
Mass/Charge, Da

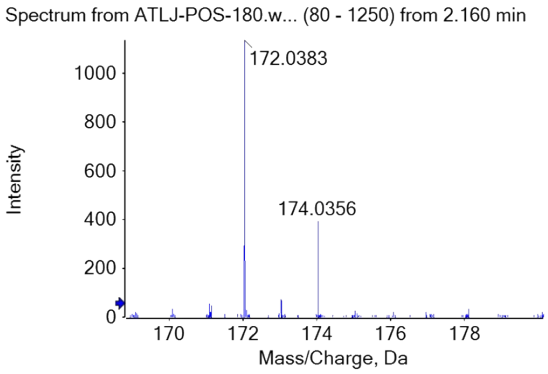
Spectrum from ATLJ-POS-180.w... (80 - 1250) from 2.160 min
172.0383
174.0356
Intensity
Mass/Charge, Da

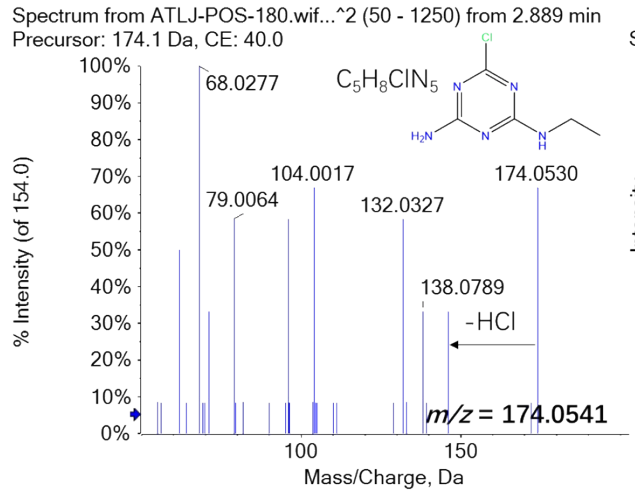
Spectrum from ATLJ-POS-180.wif...^2 (50 - 1250) from 2.889 min
Precursor: 174.1 Da, CE: 40.0
68.0277
C5H8ClN5
104.0017
174.0530
79.0064
132.0327
138.0789
-HCl
m/z = 174.0541
% Intensity (of 154.0)
Mass/Charge, Da

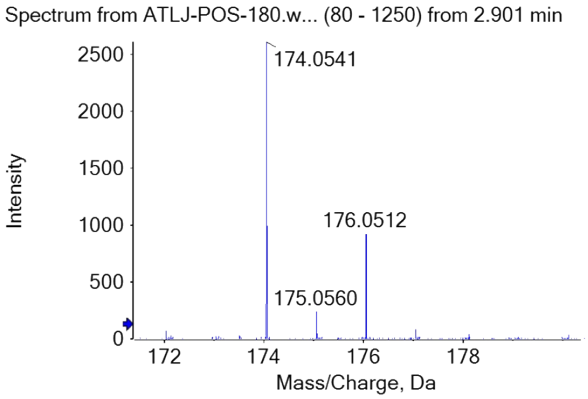
Spectrum from ATLJ-POS-180.w... (80 - 1250) from 2.901 min
174.0541
176.0512
175.0560
Intensity
Mass/Charge, Da

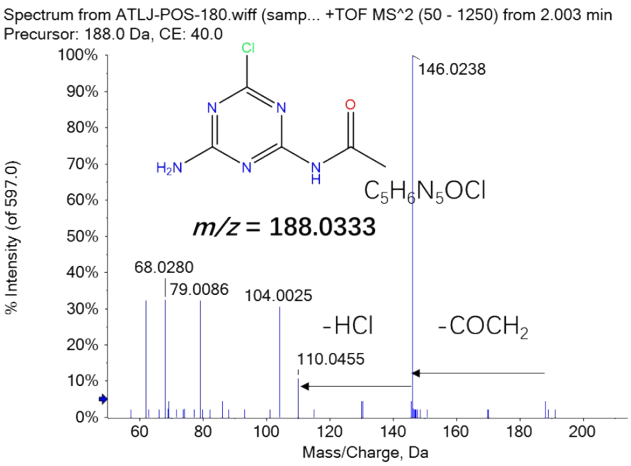
Spectrum from ATLJ-POS-180.wiff (samp... +TOF MS^2 (50 - 1250) from 2.003 min
Precursor: 188.0 Da, CE: 40.0
146.0238
C5H6N5OCl
m/z = 188.0333
68.0280
79.0086
104.0025
-HCl
-COCH2
110.0455
% Intensity (of 597.0)
Mass/Charge, Da

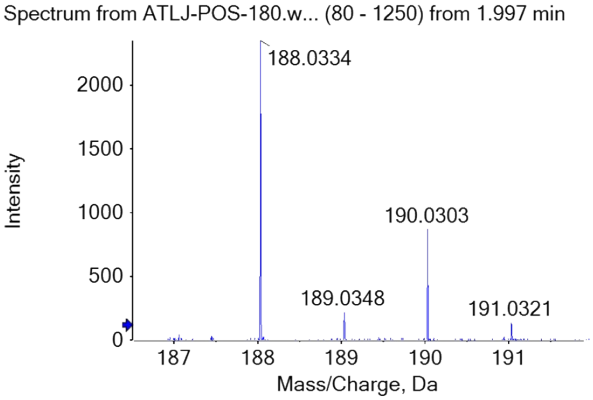
Spectrum from ATLJ-POS-180.w... (80 - 1250) from 1.997 min
188.0334
190.0303
189.0348
191.0321
Intensity
Mass/Charge, Da

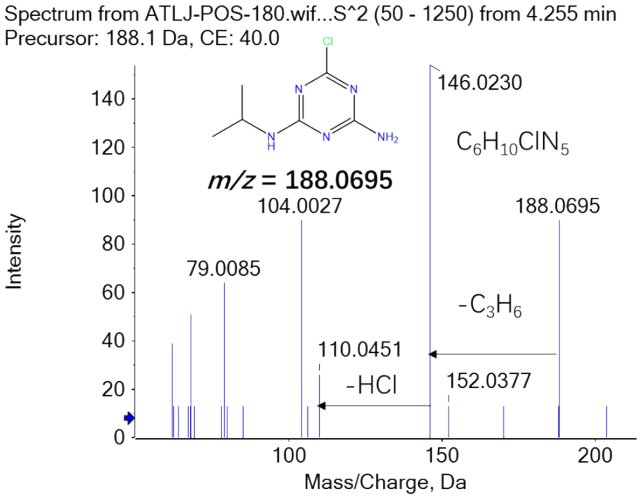
Spectrum from ATLJ-POS-180.wif...S^2 (50 - 1250) from 4.255 min
Precursor: 188.1 Da, CE: 40.0
m/z = 188.0695
C6H10ClN5
146.0230
188.0695
104.0027
79.0085
110.0451
152.0377
-C3H6
-HCl
Intensity
Mass/Charge, Da

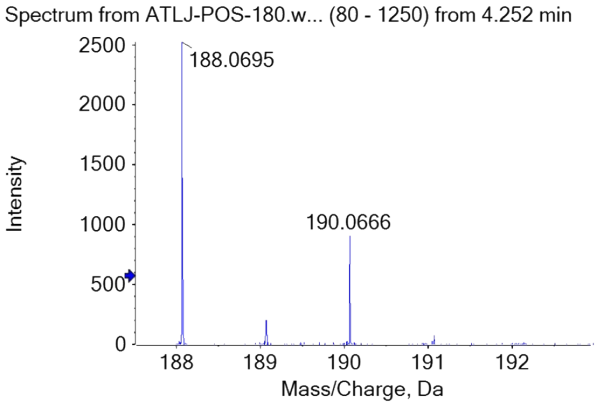
Spectrum from ATLJ-POS-180.w... (80 - 1250) from 4.252 min
188.0695
190.0666
Intensity
Mass/Charge, Da

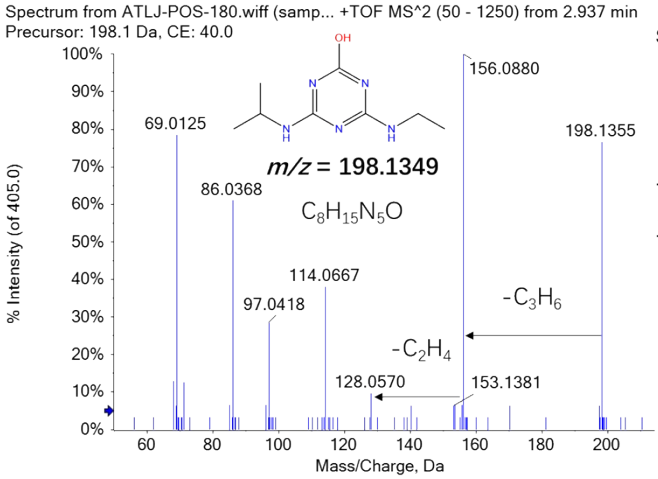
Spectrum from ATLJ-POS-180.wiff (samp... +TOF MS^2 (50 - 1250) from 2.937 min
Precursor: 198.1 Da, CE: 40.0
m/z = 198.1349
C8H15N5O
156.0880
198.1355
69.0125
86.0368
114.0667
97.0418
128.0570
153.1381
-C3H6
-C2H4
% Intensity (of 405.0)
Mass/Charge, Da

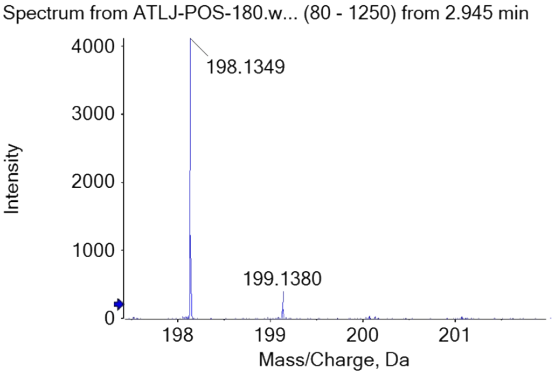
Spectrum from ATLJ-POS-180.w... (80 - 1250) from 2.945 min
198.1349
199.1380
Intensity
Mass/Charge, Da

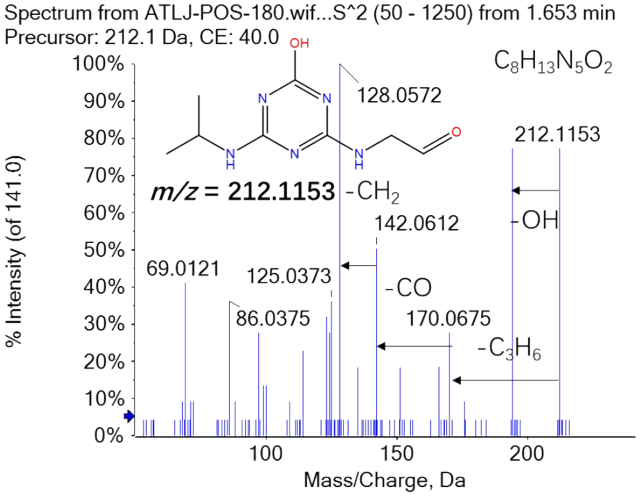
Spectrum from ATLJ-POS-180.wif...S^2 (50 - 1250) from 1.653 min
Precursor: 212.1 Da, CE: 40.0
m/z = 212.1153
C8H13N5O2
128.0572
212.1153
142.0612
69.0121
125.0373
86.0375
170.0675
-CH2
-OH
-CO
-C3H6
% Intensity (of 141.0)
Mass/Charge, Da

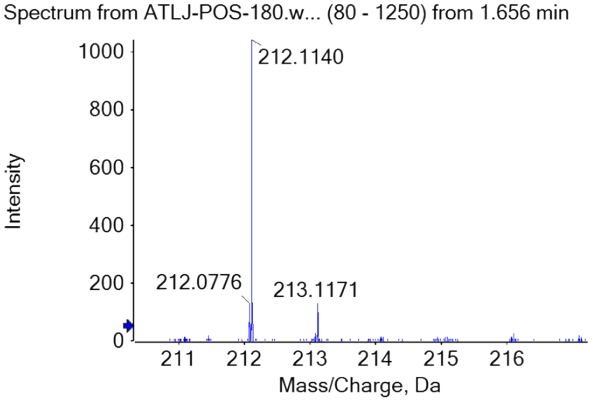
Spectrum from ATLJ-POS-180.w... (80 - 1250) from 1.656 min
212.1140
212.0776
213.1171
Intensity
Mass/Charge, Da

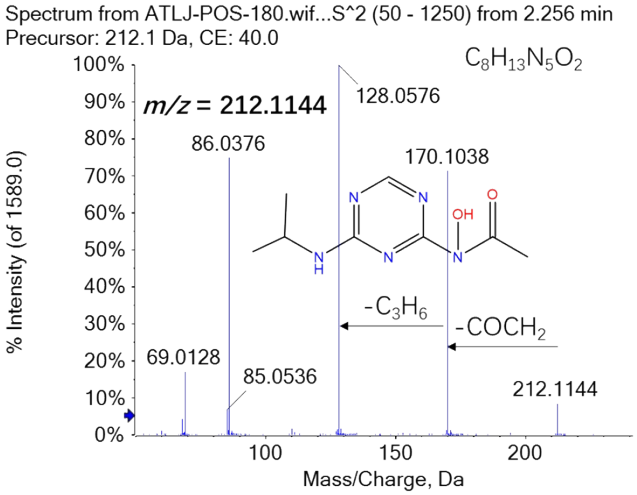
Spectrum from ATLJ-POS-180.wif...S^2 (50 - 1250) from 2.256 min
Precursor: 212.1 Da, CE: 40.0
$C_8H_{13}N_5O_2$
m/z = 212.1144
128.0576
86.0376
170.1038
-C_3H_6
-$COCH_2$
69.0128
85.0536
212.1144
% Intensity (of 1589.0)
Mass/Charge, Da

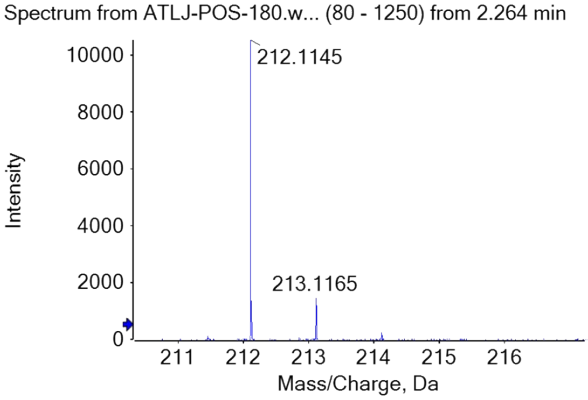
Spectrum from ATLJ-POS-180.w... (80 - 1250) from 2.264 min
212.1145
213.1165
Intensity
Mass/Charge, Da

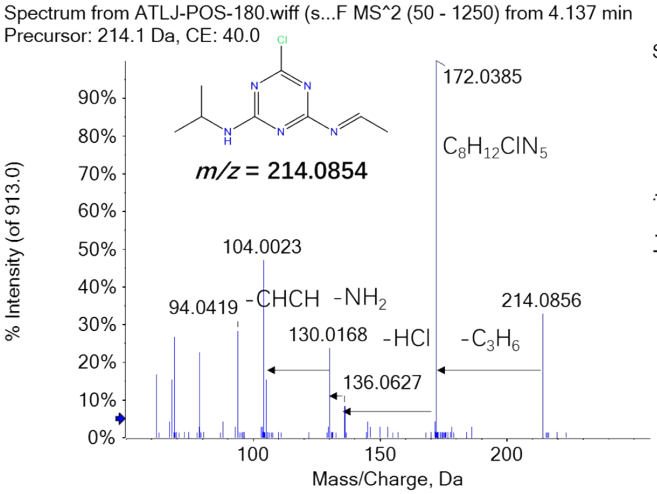
Spectrum from ATLJ-POS-180.wiff (s...F MS^2 (50 - 1250) from 4.137 min
Precursor: 214.1 Da, CE: 40.0
172.0385
$C_8H_{12}ClN_5$
m/z = 214.0854
104.0023
94.0419
-CHCH
-NH_2
214.0856
130.0168
-HCl
-C_3H_6
136.0627
% Intensity (of 913.0)
Mass/Charge, Da

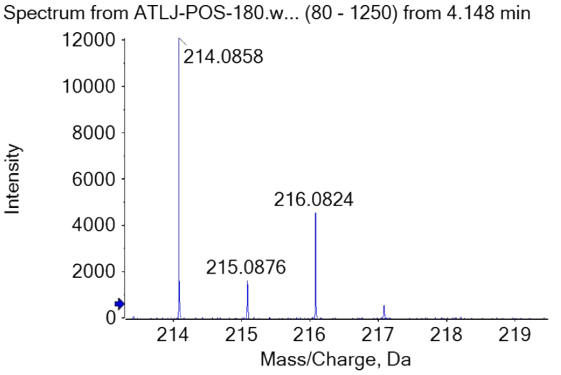
Spectrum from ATLJ-POS-180.w... (80 - 1250) from 4.148 min
214.0858
216.0824
215.0876
Intensity
Mass/Charge, Da

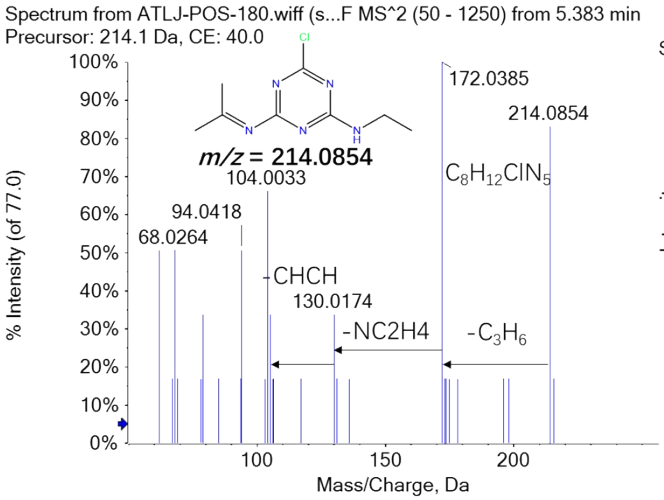
Spectrum from ATLJ-POS-180.wiff (s...F MS^2 (50 - 1250) from 5.383 min
Precursor: 214.1 Da, CE: 40.0
172.0385
214.0854
$C_8H_{12}ClN_5$
m/z = 214.0854
104.0033
94.0418
68.0264
-CHCH
130.0174
-NC2H4
-C_3H_6
% Intensity (of 77.0)
Mass/Charge, Da

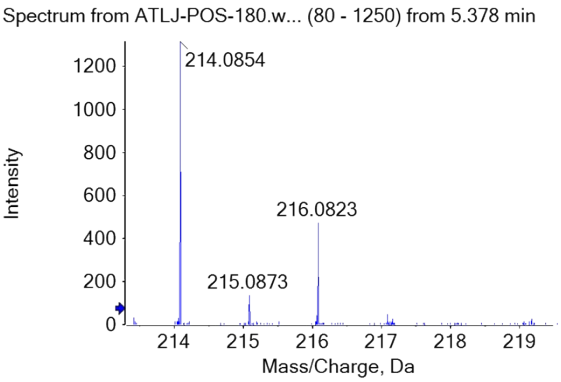
Spectrum from ATLJ-POS-180.w... (80 - 1250) from 5.378 min
214.0854
216.0823
215.0873
Intensity
Mass/Charge, Da

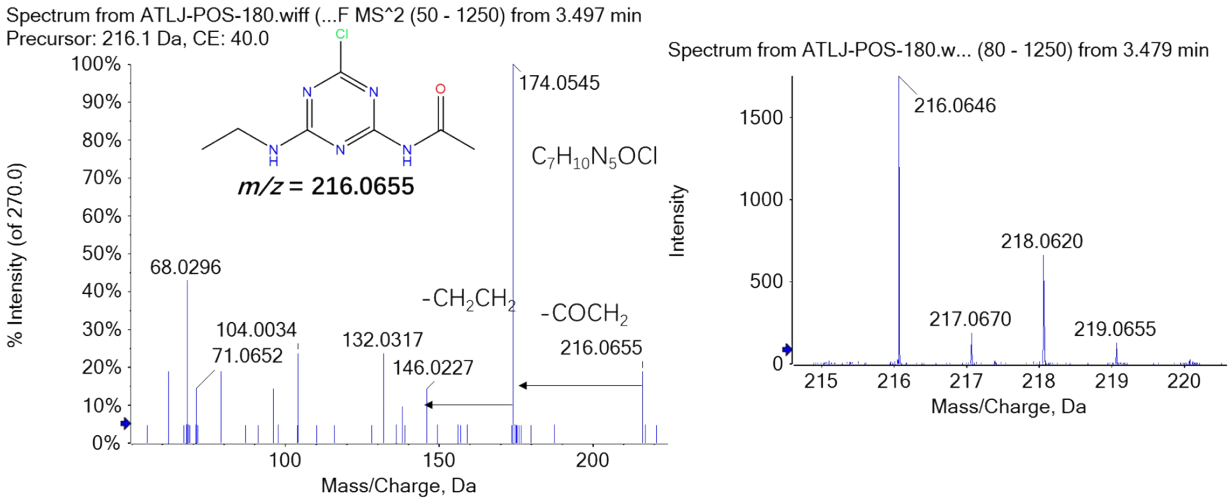
Spectrum from ATLJ-POS-180.wiff (...F MS^2 (50 - 1250) from 3.497 min
Precursor: 216.1 Da, CE: 40.0
m/z = 216.0655
C7H10N5OCl
174.0545
68.0296
104.0034
71.0652
132.0317
146.0227
216.0655
-CH2CH2
-COCH2
% Intensity (of 270.0)
Mass/Charge, Da
Spectrum from ATLJ-POS-180.w... (80 - 1250) from 3.479 min
216.0646
218.0620
217.0670
219.0655
Intensity
Mass/Charge, Da

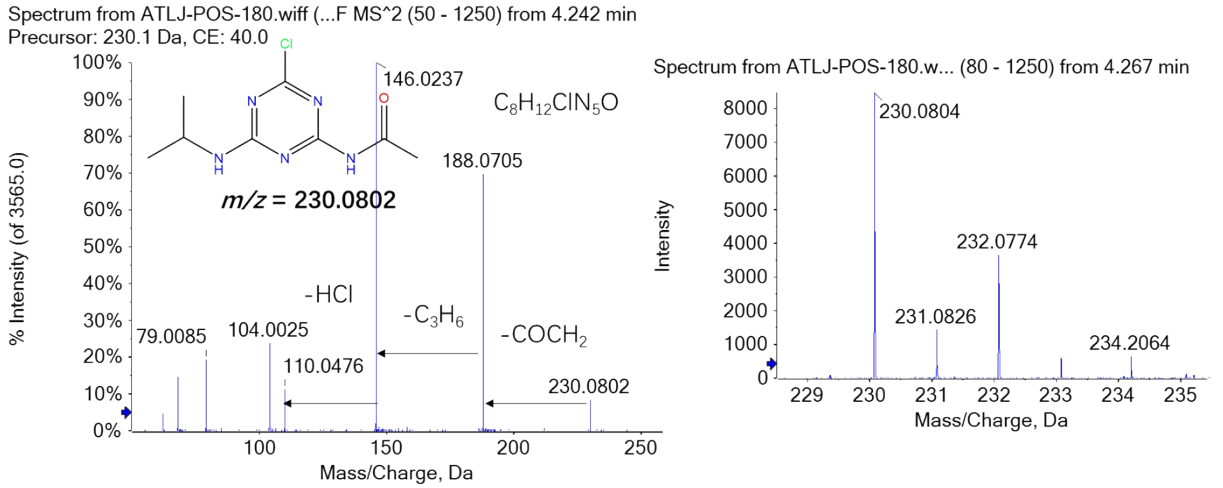
Spectrum from ATLJ-POS-180.wiff (...F MS^2 (50 - 1250) from 4.242 min
Precursor: 230.1 Da, CE: 40.0
m/z = 230.0802
C8H12ClN5O
146.0237
188.0705
79.0085
104.0025
110.0476
230.0802
-HCl
-C3H6
-COCH2
% Intensity (of 3565.0)
Mass/Charge, Da
Spectrum from ATLJ-POS-180.w... (80 - 1250) from 4.267 min
230.0804
232.0774
231.0826
234.2064
Intensity
Mass/Charge, Da

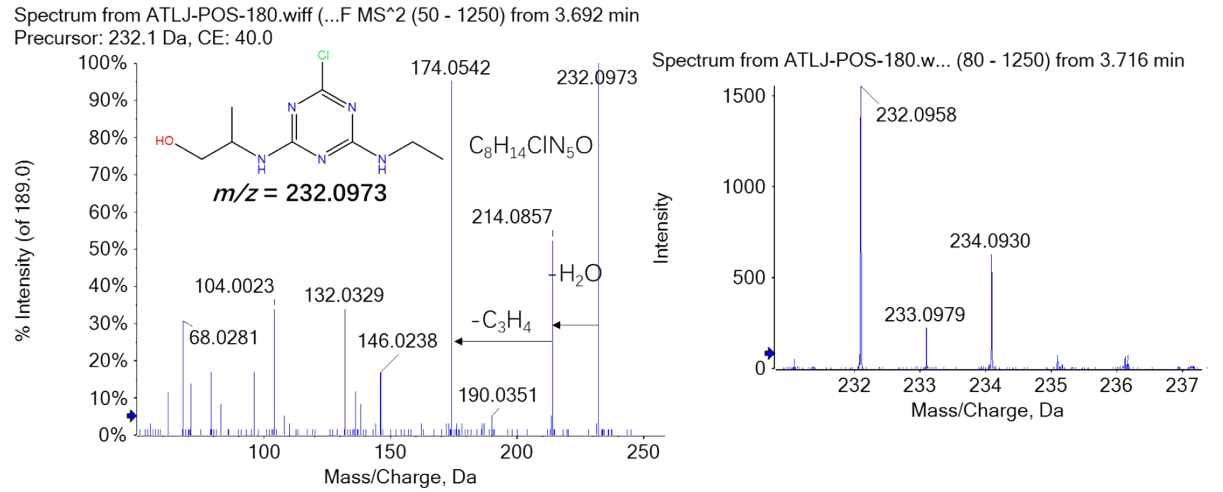
Spectrum from ATLJ-POS-180.wiff (...F MS^2 (50 - 1250) from 3.692 min
Precursor: 232.1 Da, CE: 40.0
m/z = 232.0973
C8H14ClN5O
174.0542
232.0973
214.0857
104.0023
132.0329
68.0281
146.0238
190.0351
-H2O
-C3H4
% Intensity (of 189.0)
Mass/Charge, Da
Spectrum from ATLJ-POS-180.w... (80 - 1250) from 3.716 min
232.0958
234.0930
233.0979
Intensity
Mass/Charge, Da

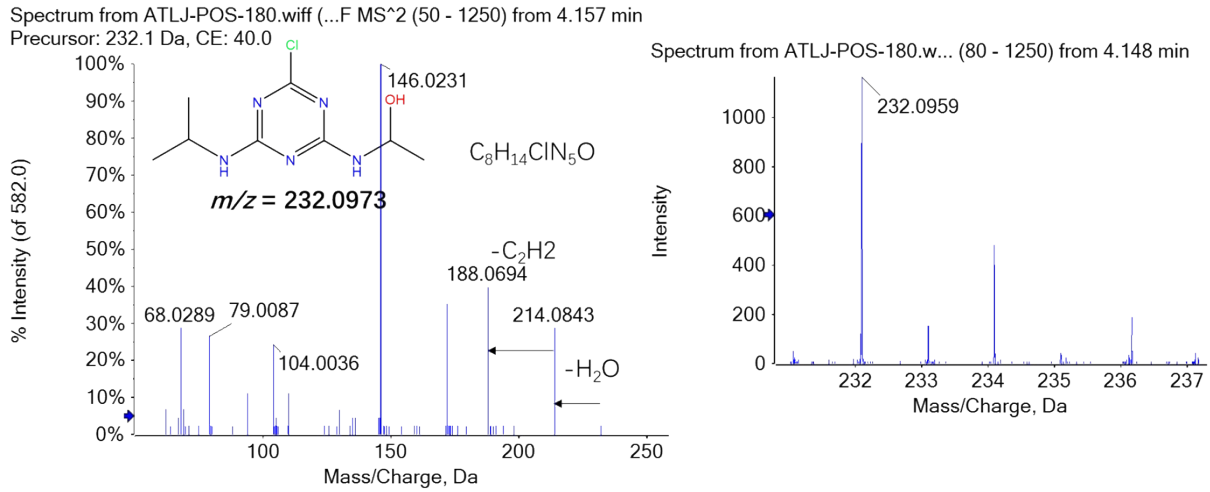

Fig. S8. MS/MS spectra of atrazine TP during UV-EC/Cl_2process. General reaction conditions: $[atrazine]_0$ = 20 µM, $[Cl^-]_0$ = 20 mM, 10 mM phosphate buffer (pH = 7.0), anodic potential = 1.5 V *vs.* Ag/AgCl, average UV_{275nm} fluence rate = 0.25 mW cm^{-2}.

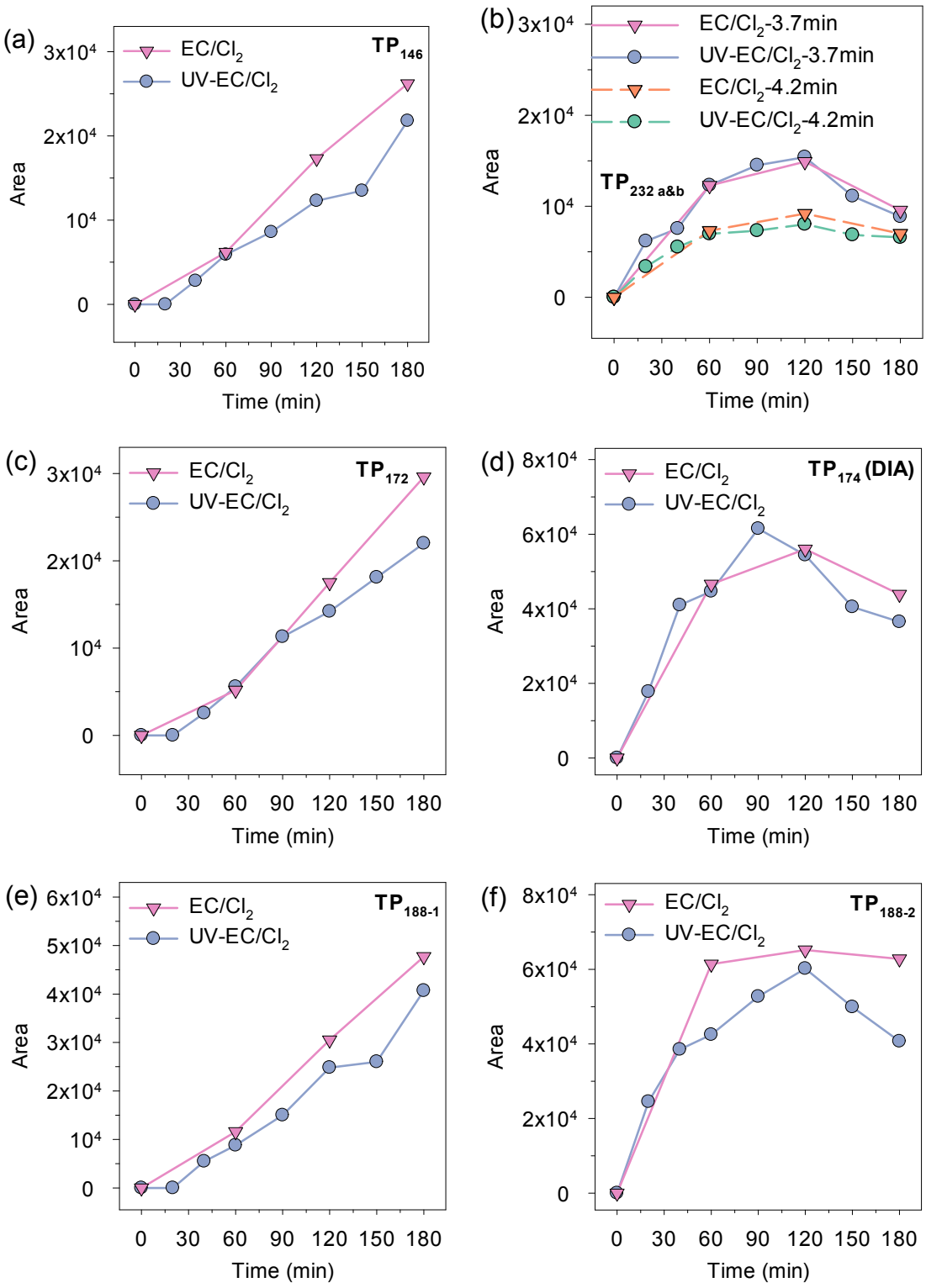
(a)
EC/Cl2
UV-EC/Cl2
TP146
Area
Time (min)
(b)
EC/Cl2-3.7min
UV-EC/Cl2-3.7min
EC/Cl2-4.2min
UV-EC/Cl2-4.2min
TP232 a&b
Area
Time (min)
(c)
EC/Cl2
UV-EC/Cl2
TP172
Area
Time (min)
(d)
EC/Cl2
UV-EC/Cl2
TP174 (DIA)
Area
Time (min)
(e)
EC/Cl2
UV-EC/Cl2
TP188-1
Area
Time (min)
(f)
EC/Cl2
UV-EC/Cl2
TP188-2
Area
Time (min)

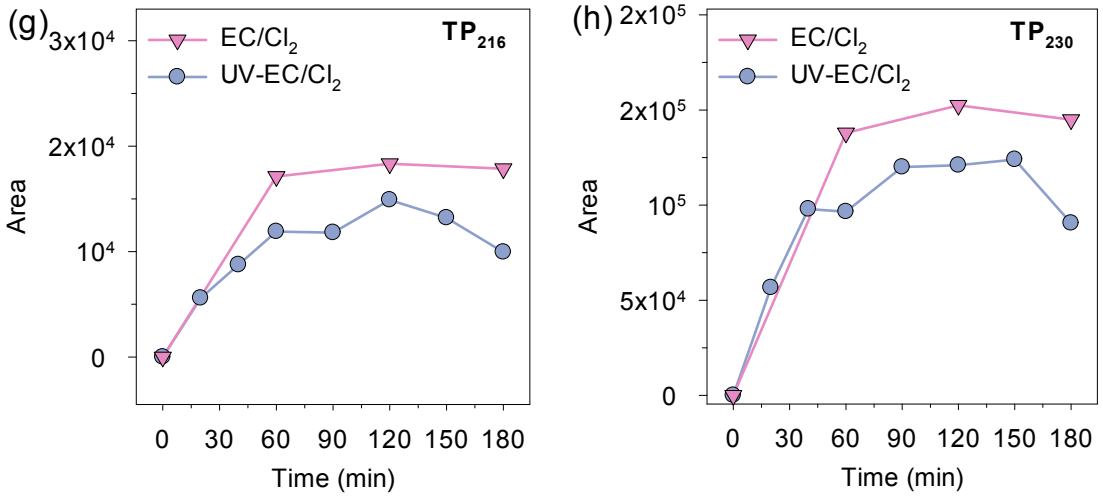

Fig. S9. Comparison of the TPs evolution *vs* time during the atrazine degradation by UV-EC/Cl_2 and EC/Cl_2, measured by QTOF-LC/MS. General reaction conditions: $[atrazine]_0$ = 20 µM, $[Cl^-]_0$ = 20 mM, 10 mM phosphate buffer (pH = 7.0), anodic potential = 1.5 V *vs.* Ag/AgCl, average UV_{275nm} fluence rate = 0.25 mW cm^{-2}.

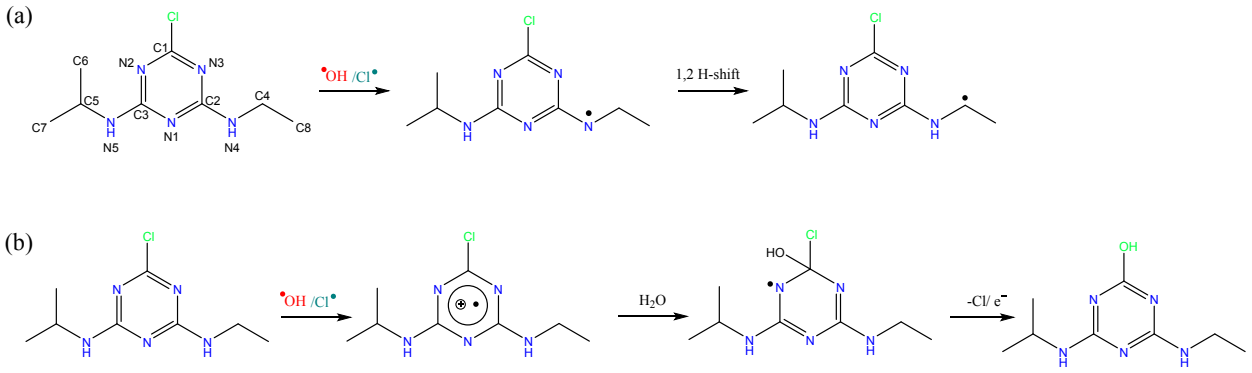

Fig. S10. Proposed mechanisms of the N-centered C-centered radicals.

References

1. M. M. Huber, S. Canonica, G.-Y. Park and U. von Gunten, Oxidation of pharmaceuticals during ozonation and advanced oxidation processes, *Environmental Science & Technology*, 2003, **37**, 1016-1024.
2. X. Kong, L. Wang, Z. Wu, F. Zeng, H. Sun, K. Guo, Z. Hua and J. Fang, Solar irradiation combined with chlorine can detoxify herbicides, *Water Research*, 2020, **177**, 115784.
3. G. V. Buxton and M. S. Subhani, Radiation chemistry and photochemistry of oxychlorine ions. Part 2.—Photodecomposition of aqueous solutions of hypochlorite ions, *Journal of the Chemical Society, Faraday Transactions 1: Physical Chemistry in Condensed Phases*, 1972, **68**, 958-969.
4. Y. Huang, M. Kong, D. Westerman, E. G. Xu, S. Coffin, K. H. Cochran, Y. Liu, S. D. Richardson, D. Schlenk and D. D. Dionysiou, Effects of HCO_3^- on degradation of toxic contaminants of emerging concern by UV/NO_3^-, *Environmental Science & Technology*, 2018, **52**, 12697-12707.
5. Y. Lei, S. Cheng, N. Luo, X. Yang and T. An, Rate constants and mechanisms of the reactions of $Cl^{\bullet}$ and $Cl_2^{\bullet-}$ with trace organic contaminants, *Environmental Science & Technology*, 2019, **53**, 11170-11182.
6. Y. Huang, Y. Liu, M. Kong, E. G. Xu, S. Coffin, D. Schlenk and D. D. Dionysiou, Efficient degradation of cytotoxic contaminants of emerging concern by UV/H2O2, *Environmental Science: Water Research & Technology*, 2018, **4**, 1272-1281.
7. Y.-y. Chen, T. Zhang, X. Wang, Y.-q. Shao and D. Tang, Phase structure and microstructure of a nanoscale TiO_2–RuO_2–IrO_2–Ta_2O_5 anode coating on titanium, *Journal of the American Ceramic Society*, 2008, **91**, 4154-4157.